





# Design of free-space couplers for suspended triangular nano-beam waveguides

J P Hadden<sup>1,2,3,\*</sup> , Cobi Maynard<sup>1,3</sup>, Daryl M Beggs<sup>1,3</sup> , Robert A Taylor<sup>4</sup>   
and Anthony J Bennett<sup>1,2,3</sup> 

<sup>1</sup> School of Physics and Astronomy, Cardiff University, Queen's Buildings, Cardiff CF24 3AA, United Kingdom

<sup>2</sup> School of Engineering, Cardiff University, Queen's Buildings, Cardiff CF24 3AA, United Kingdom

<sup>3</sup> Translational Research Hub, Cardiff University, Maindy Road, Cathays, Cardiff, CF24 4HQ, United Kingdom

<sup>4</sup> Clarendon Laboratory, Department of Physics, University of Oxford, Parks Road, Oxford OX1 3PU, United Kingdom

E-mail: [haddenj@cardiff.ac.uk](mailto:haddenj@cardiff.ac.uk)

Received 30 June 2022, revised 9 September 2022

Accepted for publication 22 September 2022

Published 5 October 2022



CrossMark

## Abstract

Photonic waveguides (WGs) with triangular cross section are being investigated for material systems such as diamond, glasses and gallium nitride, which lack easy options to create conventional rectangular nanophotonic waveguides. The design rules for optical elements in these triangular WGs, such as couplers and gratings, are not well established. Here we present simulations of elements designed to couple light into, and out of, triangular WGs from the vertical direction, which can be implemented with current angled-etch fabrication technology. The devices demonstrate coupling efficiencies approaching 50% for light focused from a high numerical aperture objective. The implementation of such couplers will enable fast and efficient testing of closely spaced integrated circuit components.

Keywords: integrated optics devices, compound semiconductors, nano photonics, Bragg reflector grating, grating coupler, free space coupler, FDTD optical modelling

(Some figures may appear in colour only in the online journal)

## 1. Introduction

Triangular waveguides (WGs) have been used to study integrated photonics with colour centres hosted in diamond [1, 2], silicon carbide [3] and also with rare earth ions in glass [4]. Angled etching of these materials creates high-index-contrast WGs, and thus tight confinement of the optical field, albeit

with geometry that is less well studied than conventional rectangular or ridge WGs. Two methods have been used to create triangular WGs: (a) Faraday cage-assisted dry-etching, which deflects the ions in an inductively coupled plasma etcher away from the surface normal, creating undercut structures in a single step by etching from both sides simultaneously as shown by Burek *et al* [2], and (b) angled focused-ion-beam etching (FIB), where sequential etching from one side, then the other, fully releases the waveguide from the surrounding material as shown by Bayn *et al* [1]. Both methods are useful for materials systems without a selective anisotropic etch that that may otherwise be used to undercut photonic devices. The latter can offer in-situ control of the waveguide position and shape, but the former

\* Author to whom any correspondence should be addressed.



Original Content from this work may be used under the terms of the [Creative Commons Attribution 4.0 licence](https://creativecommons.org/licenses/by/4.0/). Any further distribution of this work must maintain attribution to the author(s) and the title of the work, journal citation and DOI.

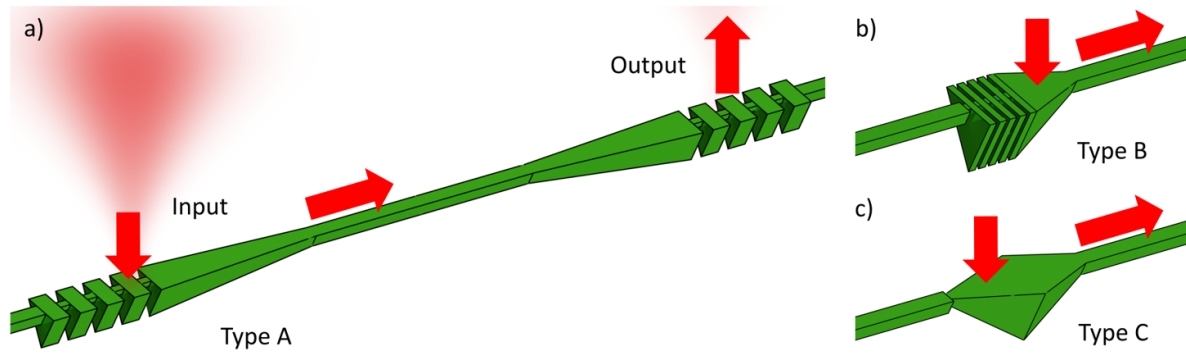


**Figure 1.** (a) Illustration of waveguide device with input and output couplers of Type A—grating coupler with mode converter. (b) Type B—wedge mirror with Bragg reflector, and (c) Type C—wedge mirror with mode converter.

is best suited to mass-manufacture of many devices in a single step.

Recently, the fabrication of suspended triangular nano-beams in gallium nitride (GaN) has been demonstrated using angled Faraday cage-assisted etching [5]. GaN is a wide band-gap compound semiconductor underpinning high-power electronics and UV–visible light sources. It has also been shown to host single photon emitters with wavelengths spanning the visible to near infra red spectrum—which is a key requirement for optical quantum technologies [6–8]. New fabrication technology can open the way towards integrated optical devices based on this versatile electro-optic material, such as low-footprint nano-lasers [9], non-linear optical light sources [10] and high speed optical switches [11, 12] with potential applications as on-chip optical interconnects.

Light may be coupled into and out of WGs using grating couplers based on periodic modulation of the effective refractive index. Such vertical couplers, as illustrated in figure 1 have important applications in the testing and development of photonic integrated circuit components, allowing for fast and efficient testing of closely spaced components. In ridge WGs, such as silicon on insulator, this is commonly achieved by etching periodic trenches into the WG. The effective refractive index is dependent on the etch depth and length of the etched sections, reducing the effective refractive index  $n_{\text{eff}}$  of the WG mode in these regions [13]. For triangular WGs, one may modify the refractive index by modulating the top WG width. Figure 1(a) shows the effective refractive indices of the first four modes in an equilateral triangular WG as a function of the WG top width width  $w$ , at 1550 nm wavelength, calculated using Ansys Lumerical Mode [14]. The first two modes may be categorised as TE-like and TM-like, while the subsequent modes appear to show rotation symmetry of order three. The nominal target waveguide size is chosen to be 765 nm, the largest size that prevents modes 3 and 4 being guided [15]. Field intensity plots of the TE and TM modes for a WG with top width of 765 nm are shown in figures 1(b) and (c).

Although there has already been considerable effort developing optimised fibre to chip couplers in conventional rectangular WG geometries [16], there has been much less on the problem of coupling light from microscope objectives

into nanophotonic waveguides in or in triangular waveguide geometries. In this work we present designs for free-space couplers based on the triangular nano-beam geometry which couple light focused from above to a Gaussian spot by a high NA microscope objective. We present three classes of designs as illustrated in figure 2: Type A—grating coupler with mode converter, Type B—wedge mirror with Bragg reflector, and Type C—wedge mirror with mode converter, with performance of the designs is evaluated and optimised using Ansys Lumerical FDTD [14]. We focus on gallium nitride as the host material. Although the refractive indices may be different, the design concepts and fabrication processes will be transferable to other material systems such as glass, diamond, silicon, silica and other compound semiconductors.

## 2. Type A coupler design—grating coupler with mode converter

The top and side profiles of a Type A vertical grating coupler designed to couple light focused from above using a 0.9 NA objective lens are shown in figures 3(a) and (b). The grating region consists of repeating sections of thicker (width  $w_1 = 2000$  nm, length  $l_1$ ) and thinner (width  $w_2 = 400$  nm, length  $l_2$ ) sections, with a mode converter (length  $l_{\text{MC}} = 7.5 \mu\text{m}$ ) allowing adiabatic transition between the thicker grating region, and the  $w_{\text{wg}} = 765$  nm WG output. The phase matching condition for a grating coupler is  $n_{\text{eff}} - n_{\text{air}} \sin(\theta) = m \lambda / a$ , where  $n_{\text{eff}}$  is the effective index of the optical mode in the grating region,  $n_{\text{air}}$  is the refractive index of air,  $\theta \approx 0^\circ$  is the target grating diffraction angle,  $m$  is the grating order number,  $\lambda$  is the wavelength of the light, and  $a = l_1 + l_2$  is the grating pitch. The effective refractive index of the optical mode in the grating region may be estimated using  $n_{\text{eff}} = \sqrt{\text{DC} n_1^2 + ((1 - \text{DC}) n_2^2)}$  for TE Modes [17], where  $n_1$  and  $n_2$  are the effective refractive indices for WG modes in the thicker ( $w_1$ ) and thinner ( $w_2$ ) sections respectively, and  $\text{DC} = l_1 / (l_1 + l_2)$  is the duty cycle of the thicker ( $w_1$ ) section. The coupling efficiency for a Gaussian source focused from above into the TE-like WG mode is calculated as a function of the grating duty cycle and grating pitch, as shown in figure 3(c). The efficiency is defined as the overlap of the normalised field

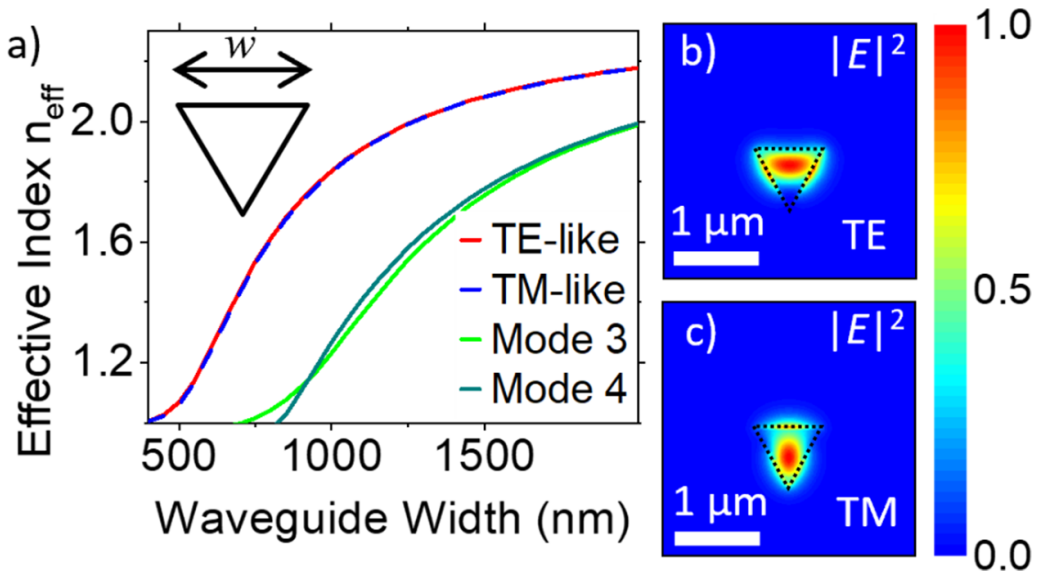


**Figure 2.** (a) Refractive index of triangular waveguides as a function of top width. (b) Electric field intensity of TE and (c) TM -like modes for a waveguide with top width of 765 nm.

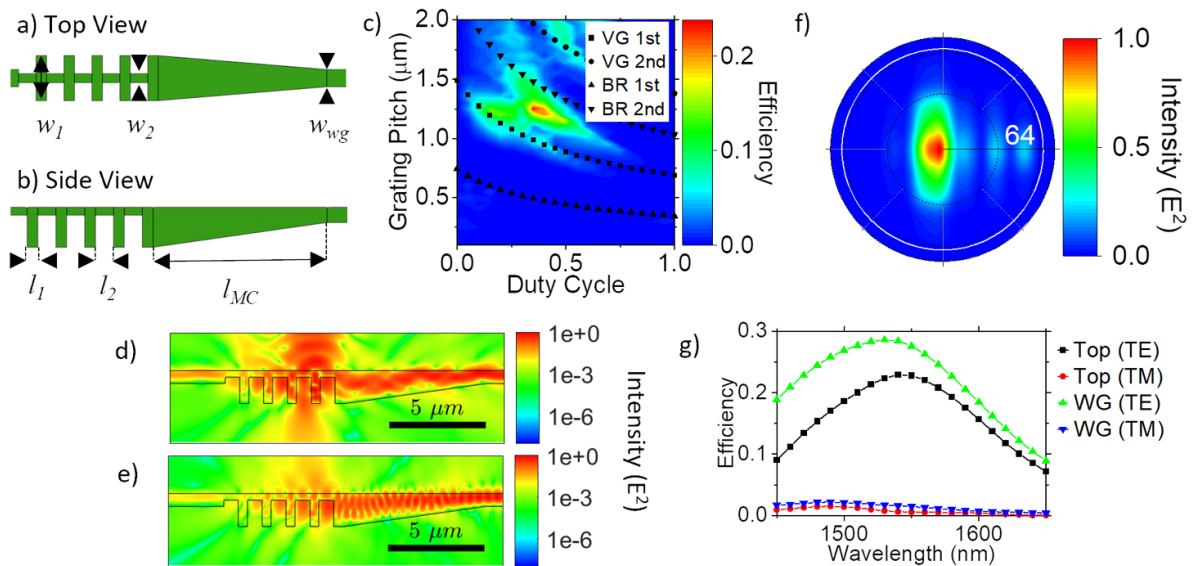


**Figure 3.** Type A coupler design (a) top and (b) side view with main design parameters marked: grating coupler widths ( $w_1$  and  $w_2$ ) and lengths ( $l_1$  and  $l_2$ ), mode converter length ( $l_{MC}$ ) and waveguide width ( $w_{wg}$ ). (c) Calculated coupling efficiency for a Gaussian source focused from above into the TE-like waveguide mode as function of duty cycle ( $l_1/(l_1 + l_2)$ ) and grating pitch ( $l_1 + l_2$ ) for a grating coupler with  $w_1 = 2000\text{nm}$  and  $w_2 = 400\text{nm}$ . The pitch and duty cycle (DC) which satisfy the 1st and 2nd order vertical grating (VG) and Bragg reflector (BR) phase matching conditions are marked as a dotted line in (c). (d) Side view cross section field intensity distribution for coupler with light input from the top and (e) through the waveguide with TE-like polarisation. (f) Far field intensity distribution with TE waveguide input source. (g) Simulated coupling efficiency as a function of wavelength for light input from the top (labelled ‘Top’) and through the waveguide (labelled ‘WG’) in TE and TM-like polarisations.

intensity with the nano-beam’s TE WG mode. The pitch and duty cycle which satisfy the 1st and 2nd order vertical grating and Bragg reflector phase matching conditions are marked as a dotted line in (c).

The most efficient design is achieved with duty cycle  $DC = 0.35$ , and grating pitch  $a = 1.25\ \mu\text{m}$ , leading to a coupling efficiency of 24%. This is modest compared to grating couplers optimised for single mode optical fibre to chip coupling in silicon on silica platforms, where theoretical

coupling efficiencies can exceed 90% [18]. However, such optical fibre grating couplers typically have dimensions comparable to the single mode fibres—orders of magnitude larger than the  $\sim 1\ \mu\text{m}^2$  focussed spot considered here, and require long tapering regions to convert from the grating coupler to the WGs. Compact grating couplers designed for microscope collection from silicon nitride WGs show more comparable theoretical coupling efficiencies of up to 40% (or 60% when including a reflective mirror underneath) [19].

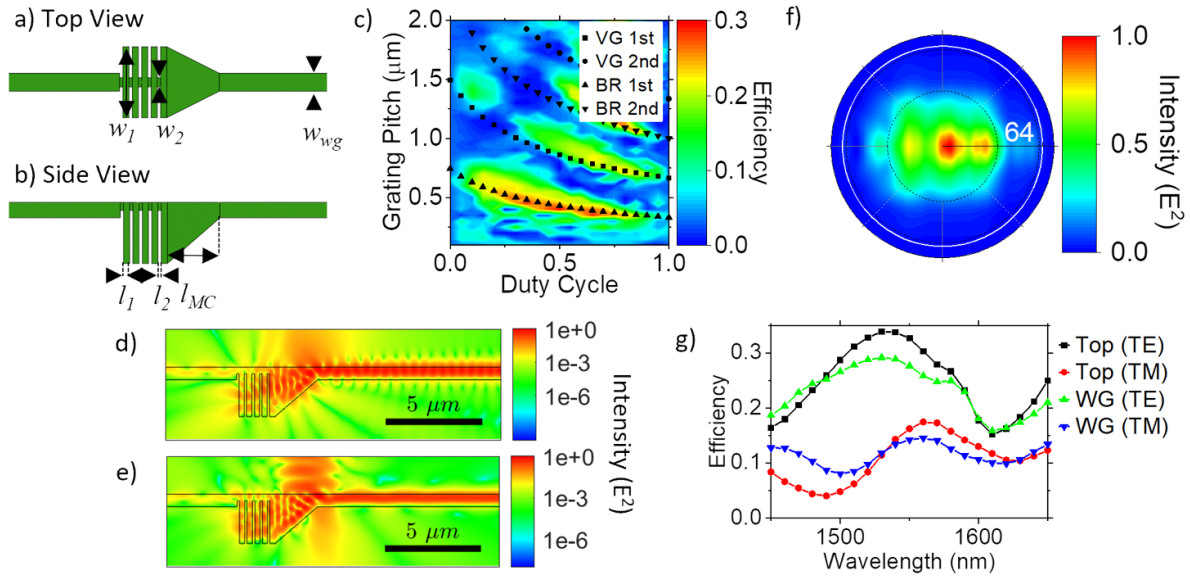


**Figure 4.** Type B coupler design (a) top and (b) side view with main design parameters marked: grating coupler widths ( $w_1$  and  $w_2$ ) and lengths ( $l_1$  and  $l_2$ ), mode converter length ( $l_{MC}$ ) and waveguide width ( $w_{wg}$ ). (c) Calculated efficiency of coupling a Gaussian source focused from above into the TE-like waveguide mode as function of duty cycle ( $l_1/(l_1 + l_2)$ ) and grating pitch ( $l_1 + l_2$ ) for a grating coupler with  $w_1 = 3000\text{nm}$  and  $w_2 = 400\text{nm}$ . The pitch and duty cycle which satisfy the vertical grating and Bragg reflector phase matching conditions are marked. (d) Side view cross section field intensity distribution for coupler with focused Gaussian TE input and (e) with TE waveguide input sources. (f) Far field intensity distribution with TE waveguide input. (g) Simulated coupling efficiency as a function of wavelength for light input from the top (Top) and through the waveguide in TE and TM-like polarisations.

Interestingly, this design does not appear to satisfy the grating coupler phase matching condition. Designs which do are limited to around 15%. We believe the reason that this design outperforms grating designs that satisfy the phase matching condition is that the size of focused the Gaussian spot is only large enough to cover one period of the grating, and thus, the device is exhibiting a Mie resonance which is enhancing the coupling—as recently shown in silicon nanowire super-lattices [20]. Grating couplers which demonstrate out-coupling from a single period have also been demonstrated in gallium arsenide for out coupling quantum dot emission [21].

The grating coupler design was further optimised using a particle swarm algorithm, varying the grating pitch, duty cycle, and the offset of the focused source TE polarised source. The resulting solution was then evaluated using four different input scenarios: Top (TE) focused Gaussian input with TE-like polarisation—where the electric field is perpendicular to the waveguide, Top (TM) focused Gaussian input with TM-like polarisation—where the electric field parallel is to the WG, WG (TE) input through the WG TE-like mode, WG (TM) input through the WG TM-like mode. This allows us to test how the optimised coupler performs to couple light from free-space into the WG, and conversely from the WG into free-space in both TE and TE-like polarisations. Figure 3(d) shows the field intensity of a cross section of the optimised grating coupler when illuminated from above with a TE source, demonstrating how the field is coupled from a focused Gaussian source above the grating region, to the WG output on the right hand side, while figure 3(d) shows the shows the field intensity when the WG is excited through the WG mode,

while figure 3(f) shows a far field projection of the output of the coupler in the vertical direction. We can estimate the collection efficiency of this output into a microscope objective by integrating the field intensity within the angular cone defined by a 0.9 NA collection objective ( $\theta = 64^\circ$ ). The performance of the coupler for both TE and TM-like modes from the four different input scenarios over a wavelength range of 200 nm around the 1550 nm design wavelength is shown in figure 3(g). It can be seen that the device performs well for TE-like modes with peak efficiencies of 23% for top illumination, 28% for WG illumination with a bandwidth of around 200 nm, however for TM polarised light efficiencies peak at less than 2%.

### 3. Type B coupler design: wedge mirror with Bragg reflector

During optimisation of the type A design it was discovered that for certain lengths of  $l_{MC}$  the mode converter section of the waveguide actually performs as an angled mirror, allowing light to be reflected through total internal reflection from the vertical direction to the horizontal. Rectangular total internal reflection mirror couplers have previously been demonstrated in diamond through focused ion beam milling [22]. However, the triangular geometry investigated here presents a tapered ‘wedge mirror’ shape. When combined with a Bragg reflector, it is possible to design a device which reflects and directs light focused from above into the the waveguide mode.

Figures 4(a) and (b) show the top and side profiles of a Type B device combining a wedge mirror and a Bragg reflector.

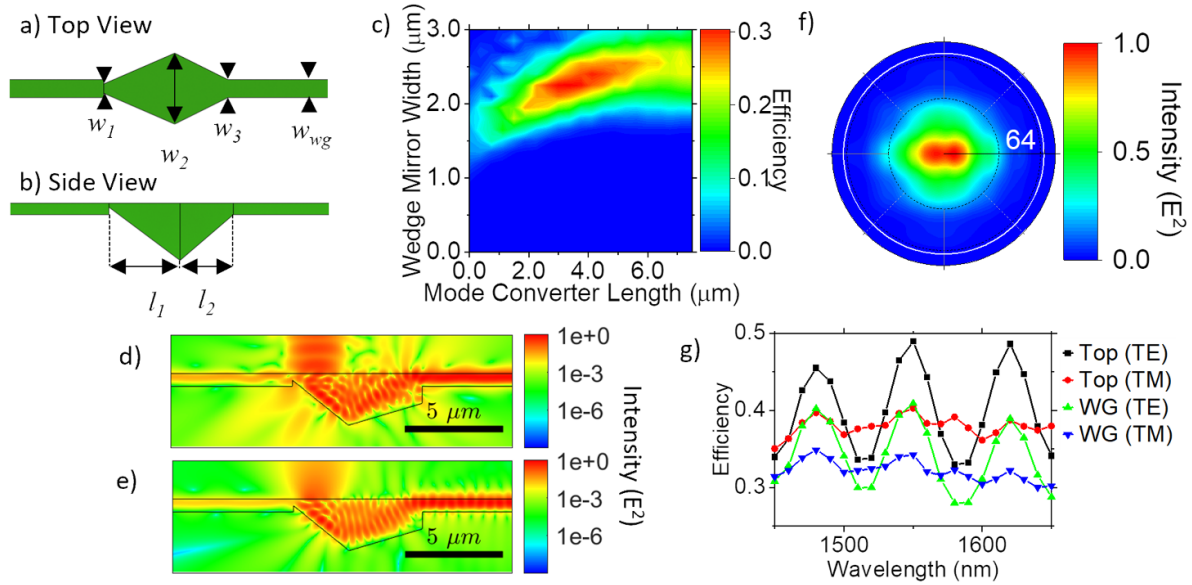


**Figure 5.** Type C coupler design (a) top and (b) side view with main design parameters marked: wedge mirror and mode converter lengths ( $w_1$ ,  $w_2$ ,  $w_3$ ) and lengths ( $l_1$ ,  $l_2$ ) and waveguide width ( $w_{wg}$ ). (c) Calculated efficiency of coupling a Gaussian source focused from above into the TE-like waveguide mode as function of mode converter length and wedge mirror width with  $w_1 = 400$  nm and  $w_3 = 765$  nm (d) Side view cross section field intensity distribution for coupler with focused Gaussian TE input and (e) with TE waveguide input sources. (f) Far field intensity distribution with TE waveguide input source. (g) Coupling efficiency of coupler as a function of wavelength with focused Gaussian, and waveguide TE and TM like input sources.

Bragg reflectors based on modulating the waveguide width can be implemented in a similar way to the grating couplers, however in this case the phase matching condition becomes  $n_{eff} = 2(m + 1) \lambda / 2a$ . The grating region consists of repeating sections of thicker (width  $w_1 = 3000$  nm, length  $l_1$ ) and thinner (width  $w_2 = 400$  nm, length  $l_2$ ) sections, with a wedge mirror (length  $l_{MC} = 2.25 \mu\text{m}$ ) allowing total internal reflection of the focused beam from above, and directing the reflected light into the  $w_{wg} = 765$  nm waveguide output.

Figure 4(c) shows the coupling efficiency of a Gaussian source focused from above into the TE-like WG mode as a function of the grating duty cycle, and grating pitch. The pitch and duty cycle which satisfy the vertical grating and Bragg reflector phase matching conditions are marked as a dotted line in (c). It can be seen that the most efficient designs run along the Bragg reflector first order line as expected, with the best design parameters  $DC = 0.5$  and grating pitch  $a = 0.4 \mu\text{m}$  showing efficiency of 30%. It is notable that this is higher than the best Type A grating coupler design even though it combines two reflective elements.

Following a similar procedure as for the previous design, we optimise the coupling efficiency by varying the grating pitch, duty cycle, wedge mirror length and the offset of the device with respect to the focused source TE polarised source. We then evaluate the performance of the optimised coupler device as before for TE and TM polarised light for in-coupling a focused Gaussian beam from above into the WG mode (Top (TE) and Top (TM)), and for out-coupling the WG modes into a 0.9 NA collection cone representing a microscope objective (WG (TE) and WG (TM)). Figures 4(d) and (e), show the field intensity cross sections for the Top (TE) and WG (TE) scenarios respectively, while 4(f) shows the far field projection of

the field intensity for the out coupled mode. Figure 4(g) shows the performance of the device over a 200 nm wavelength range around the design wavelength.

The peak efficiency of this Type B design is 35% for top illumination, and 29% for WG illumination for TE polarised light, which is better than the Type A design. It also performs better than the Type A design for TM polarised light, with peak efficiencies of 17% and 14% respectively for Top (TM) and WG (TM) input scenarios, and spatially it is much more compact—with a total length of  $4.2 \mu\text{m}$  as compared to  $13.8 \mu\text{m}$  for design A, however the efficiency profile over the wavelength range, and the output mode are both more complex, indicating several output modes, which is less desirable for some applications—for example where the output needs to be coupled into a single mode fibre.

#### 4. Type C coupler design: wedge mirror with mode converter

The third design we consider, Type C, consists of a wedge mirror combined with a mode converter. This design uses only wedged mirrors and mode converters, with geometry controlled by their relative widths. Figures 5(a) and (b) show the top and side profiles of the Type C device, combining a wedge mirror with widths ( $w_1 = 400$  nm and  $w_2 = 3000$  nm) and length  $l_1$  and a mode converter with widths ( $w_2 = 3000$  nm and  $w_3 = 765$  nm) and length  $l_2$ . Figure 5(c) shows the coupling efficiency of a Gaussian source focused from above as the mode converter length ( $l_2$ ) and wedge mirror/mode converter thicker width ( $w_2$ ) length are varied. The highest efficiency design is obtained with  $l_2 = 3.75 \mu\text{m}$  and  $w_2 = 2.25 \mu\text{m}$ .

Subsequently, we optimise the design, allowing the wedge mirror output width ( $w_2$ ), and length ( $l_1$ ), and mode converter output width ( $w_2$ ) and length ( $l_2$ ), along with the offset of the device with respect to the focused Gaussian TE polarised source to be varied. This yields a device with a peak coupling efficiency of 49% for a focused Gaussian TE beam. Interestingly, the highest efficiency design presents a step discontinuity between the mode converter and the output WG. This device shows good performance both for in-coupling (figure 5(d)) and out coupling (figure 5(e)), with a concentrated far field projection field intensity distribution (figure 5(f)). It can also be seen in figure 5(g) that although there are some spectral resonances visible, the device works relatively well for both TE and TM polarised light, in both in-coupling and out-coupling configurations, with coupling efficiencies greater than 26% for all configurations across the range.

## 5. Conclusion

In this work, we present the design of free space couplers for suspended triangular nano-beam WGs. We investigate three different designs which demonstrate grating coupler, Bragg reflector, and total internal reflection elements, using the suspended triangular WG geometry. The optimised device designs demonstrate simulated coupling efficiencies approaching 50% for light focussed from a high numerical aperture objective. Verification of the performance of physical devices may be achieved through transmission measurements of WG devices with couplers at either end. This will be performed on devices fabricated in gallium nitride using angled Faraday cage-assisted etching and will form the basis of a future work. The development of such couplers will enable fast and efficient testing of closely spaced integrated circuit components.

## Data availability statement

The data that support the findings of this study are openly available at the following URL/DOI: <http://doi.org/10.17035/d.2022.0214949311>.

## Acknowledgments

This work was performed using the computational facilities of the Advanced Research Computing @ Cardiff (ARCCA) Division, Cardiff University. We acknowledge financial support provided by EPSRC via Grant No. EP/T017813/1 and EP/P006973/1. CM is partially funded by EP/S024441/1.

## ORCID iDs

J P Hadden  <https://orcid.org/0000-0001-5407-6754>  
 Daryl M Beggs  <https://orcid.org/0000-0002-2231-7514>  
 Robert A Taylor  <https://orcid.org/0000-0003-2578-9645>  
 Anthony J Bennett  <https://orcid.org/0000-0002-5386-3710>

## References

- [1] Bayn I, Meyler B, Salzman J and Kalish R 2011 Triangular nanobeam photonic cavities in single-crystal diamond *New J. Phys.* **13** 025018
- [2] Burek M J, de Leon N P, Shields B J, Hausmann B J M, Chu Y, Quan Q, Zibrov A S, Park H, Lukin M D and Lončar M 2012 Free-standing mechanical and photonic nanostructures in single-crystal diamond *Nano Lett.* **12** 6084–9
- [3] Majety S, Norman V A, Li L, Bell M, Saha P and Radulaski M 2021 Quantum photonics in triangular-cross-section nanodevices in silicon carbide *J. Phys. Photonics* **3** 034008
- [4] Ruskuc A, Wu C-J, Rochman J, Choi J and Faraon A 2022 Nuclear spin-wave quantum register for a solid-state qubit *Nature* **602** 408–13
- [5] Gough G P, Sobiesierski A D, Shabbir S, Thomas S, Beggs D M, Taylor R A and Bennett A J 2020 Faraday-cage-assisted etching of suspended gallium nitride nanostructures *AIP Adv.* **10** 055319
- [6] Berhane A M *et al* 2017 Bright room-temperature single-photon emission from defects in gallium nitride *Adv. Mater.* **29** 1605092
- [7] Zhou Y, Wang Z, Rasmita A, Kim S, Berhane A, Bodrog Z, Adamo G, Gali A, Aharonovich I and Gao W-B 2018 Room temperature solid-state quantum emitters in the telecom range *Sci. Adv.* **4** eaar3580
- [8] Bishop S G, Hadden J P, Hekmati R, Cannon J K, Langbein W W and Bennett A J 2022 Enhanced light collection from a gallium nitride color center using a near index-matched solid immersion lens *Appl. Phys. Lett.* **120** 114001
- [9] Niu N, Woolf A, Wang D, Zhu T, Quan Q, Oliver R A and Hu E L 2015 Ultra-low threshold gallium nitride photonic crystal nanobeam laser *Appl. Phys. Lett.* **106** 1–6
- [10] Rahmani M *et al* 2018 Nonlinear frequency conversion in optical nanoantennas and metasurfaces: materials evolution and fabrication *Opto-Electron. Adv.* **1** 18002101–12
- [11] Cuniot-Ponsard M, Saraswati I, Ko S-M, Halbwax M, Cho Y H and Dogheche E 2014 Electro-optic and converse-piezoelectric properties of epitaxial GaN grown on silicon by metal-organic chemical vapor deposition *Appl. Phys. Lett.* **104** 101908
- [12] Ying Z and Soref R 2021 Electro-optical logic using dual-nanobeam Mach-Zehnder interferometer switches *Opt. Express* **29** 12801
- [13] Marchetti R, Lacava C, Khokhar A, Chen X, Cristiani I, Richardson D J, Reed G T, Petropoulos P and Minzioni P 2017 High-efficiency grating-couplers: demonstration of a new design strategy *Sci. Rep.* **7** 16670
- [14] Lumerical Inc. (available at: <https://optics.ansys.com/hc/en-us/articles/1500007184901-Lumerical-Citation-Instruction>)
- [15] Maynard C, Hadden J P, Beggs D M, Wale Michael J, and Bennett A J 2022 Design of suspended triangular waveguides and serrated photonic crystal nanobeam cavities (in preparation)
- [16] Cheng L, Mao S, Li Z, Han Y and Fu H 2020 Grating couplers on silicon photonics: design principles, emerging trends and practical issues *Micromachines* **11** 666
- [17] Zhang J, Yang J, Lu H, Wu W, Huang J and Chang S 2015 Subwavelength TE/TM grating coupler based on silicon-on-insulator *Infrared Phys. Technol.* **71** 542–6
- [18] Bozzola A, Carroll L, Gerace D, Cristiani I and Andreani L C 2015 Optimising apodized grating couplers in a pure SOI platform to  $-0.5$  dB coupling efficiency *Opt. Express* **23** 16289

- [19] Zhu Y, Wang J, Xie W, Tian B, Li Y, Brainis E, Jiao Y and Van Thourhout D 2017 Ultra-compact silicon nitride grating coupler for microscopy systems *Opt. Express* **25** 33297
- [20] Kim S, Kim K-H, Hill D J, Park H-G and Cahoon J F 2018 Mie-coupled bound guided states in nanowire geometric superlattices *Nat. Commun.* **9** 2781
- [21] Faraon A, Fushman I, Englund D, Stoltz N, Petroff P and Vuckovic J 2008 Dipole induced transparency in waveguide coupled photonic crystal cavities *Opt. Express* **16** 12154
- [22] Castelletto S *et al* 2011 Diamond-based structures to collect and guide light *New J. Phys.* **13** 025020